Engineering and Characterization of a NADPH-Utilizing Cytochrome b_5 Reductase†

Christopher C. Marohnic,‡ Maria C. Bewley,§ and Michael J. Barber*,‡

Department of Biochemistry and Molecular Biology, University of South Florida, College of Medicine, Tampa, Florida 33612, and Biology Department, Brookhaven National Laboratory, Upton, New York 11973

Received May 19, 2003; Revised Manuscript Received July 28, 2003

ABSTRACT: Microsomal cytochrome b_5 reductase (EC 1.6.2.2) catalyzes the reduction of ferricytochrome b_5 using NADH as the physiological electron donor. Site-directed mutagenesis has been used to engineer the soluble rat cytochrome b_5 reductase diaphorase domain to utilize NADPH as the preferred electron donor. Single and double mutations at residues D239 and F251 were made in a recombinant expression system that corresponded to D239E, S and T, F251R, and Y, D239S/F251R, D239S/F251Y, and D239T/F251R, respectively. Steady-state turnover measurements indicated that D239S/F251Y was bispecific while D239T, D239S/F251R, and D239T/F251R were each NADPH-specific. Wild-type (WT) cytochrome b_5 reductase showed a 3700-fold preference for NADH whereas the mutant with the highest NADPH efficiency, D239T, showed an 11-fold preference for NADPH, a 39200-fold increase. Wild-type cytochrome b_5 reductase only formed a stable charge-transfer complex with NADH while D239T formed complexes with both NADH and NADPH. The rates of hydride ion transfer, determined by stopped-flow kinetics, were $k^{\mathrm{NADH-WT}} = 130\ s^{-1}$, $k^{\mathrm{NADPH-WT}} = 5\ s^{-1}$, $k^{\mathrm{NADH-D239T}} = 180\ s^{-1}$, and $k^{\mathrm{NADPH-D239T}} = 73\ s^{-1}$. K_s determinations by differential spectroscopy demonstrated that D239T could bind nonreducing pyridine nucleotides with a phosphate or a hydroxyl substituent at the 2′ position, whereas wild-type cytochrome b_5 reductase would only bind 2′ hydroxylated molecules. Oxidation−reduction potentials ($E°'$, $n = 2$) for the flavin cofactor were WT = −268 mV, D239T = −272 mV, WT+NAD^+ = −190 mV, D239T+NAD^+ = −206 mV, WT+$NADP^+$ = −253 mV, and D239T+$NADP^+$ = −215 mV, which demonstrated the thermodynamic contribution of $NADP^+$ binding to D239T. The crystal structures of D239T and D239T in complex with NAD^+ indicated that the loss of the negative electrostatic surface that precluded 2′ phosphate binding in the wild-type enzyme was primarily responsible for the observed improvement in the use of NADPH by the D239T mutant.

Cytochrome b_5 reductase (CB5R,[1] EC 1.6.2.2), an enzyme involved in the operation of microsomal and cytosolic electron transport systems, catalyzes the reduction of cytochrome b_5 using reduced nicotinamide adenine dinucleotide (NADH) as the physiological electron donor. The rate-limiting step of the reduction reaction has been identified as hydride ion transfer from NADH to the enzyme's flavin adenine dinucleotide (FAD) prosthetic group (*1*, *2*). The subsequent steps in the reaction sequence proceed rapidly as electrons are transferred sequentially from the reduced FAD to the heme prosthetic group of each of two molecules of ferricytochrome b_5. The product, ferrocytochrome b_5, acts as a key component in several cellular pathways by providing reducing equivalents for processes that include fatty acid elongation and desaturation (*3*), cholesterol biosynthesis (*4*), methemoglobin reduction (*5*), and steroid and xenobiotic transformations (*6*).

Rat CB5R contains a FAD binding domain comprised of amino acids L25-L147[2] and a NADH binding domain, spanning residues V171−F300, bridged by a short three-stranded antiparallel β-sheet "hinge" region, comprised of residues L148 to T170. The microsomal CB5R isoform, expressed as the major isoform in nonerythroid tissues, contains an additional 25 residue amino-terminal membrane-anchoring domain. The FAD binding domain of CB5R is a six-stranded antiparallel β-barrel capped with a single α-helix together with a long flexible loop known as the "lid" that forms the majority of contacts to the flavin ADP moiety. This domain contains several highly conserved amino acid residues that form critical contacts with the FAD on the side of the *si*-face of the isoalloxazine ring (*7*, *8*). The NADH binding domain of CB5R can be categorized as a

† This work was supported by Grants GM 32696 from the National Institutes of Health and 9701708 and 9910034V from the American Heart Association, Florida/Puerto Rico Affiliate (MJB), and DoE LDRD number 00-43 (MCB).

* To whom correspondence should be addressed. Michael J. Barber, D.Phil., University of South Florida, College of Medicine, Department of Biochemistry & Molecular Biology, 12901 Bruce B. Downs Blvd., MDC Box 7, Tampa, FL 33612. E-mail: mbarber@hsc.usf.edu. Phone: (813) 974-9702. Fax: (813) 974-7357.

‡ University of South Florida.

§ Brookhaven National Laboratory.

[1] Abbreviations: CB5R, cytochrome b_5 reductase; CD, circular dichroism; CPR, cytochrome P450 reductase; FNR, ferredoxin:$NADP^+$ reductase; FPLC, fast protein liquid chromatography; IPTG, isopropyl β-D-thioglucopyranoside; MALDI-TOF, matrix-assisted laser desorption ionization time-of-flight; μ, ionic strength; NAD(P)H:FR, NAD(P)H: ferricyanide reductase; NOS, nitric oxide synthase; NR, nitrate reductase; PAGE, polyacrylamide gel electrophoresis; PCR, polymerase chain reaction; SDS, sodium dodecyl sulfate; TB, terrific broth.

[2] Amino acid residues are numbered with respect to their position in the sequence of the full-length, membrane binding form of cytochrome b_5 reductase.

10.1021/bi034819b CCC: $25.00
Published on Web 09/05/2003

"Rossmann" type nucleotide binding fold formed by a five-stranded parallel β-sheet (*9*). This domain makes contacts with the *re*-face of the FAD and contains several conserved residues and signature motifs that form the surfaces that direct NADH binding in an appropriate conformation. Those residues that form the ADP binding site within the pyridine nucleotide binding surface are of particular interest for this pyridine nucleotide specificity study, whereby binding of 2′ hydroxylated molecules is compared to binding of 2′ phosphorylated molecules. The previously published 2.3 Å resolution crystal structure of the CB5R−NAD^+ complex (*10*) revealed that the pyridine nucleotide bound in an extended conformation across the surface formed by prolines 275 and 276, and within an ~6 Å wide channel bordered on one side by the aromatic ring of phenylalanine 251 and on the opposite side by proline 277. Aspartic acid 239 is of particular interest because of the hydrogen bond its carbonyl oxygen generates with the 2′ hydroxyl group of the pyridine nucleotide. Several additional residues form hydrogen bonds with the NAD^+ phosphate oxygens, including lysine 110 and glutamine 210.

Primary sequence homologies, including conserved FAD and NAD(P)(H) binding motifs, together with the classical two domain structural arrangement are defining features of members of the NAD(P)(H)-dependent flavoprotein transhydrogenase family named for the prototypical enzyme ferredoxin:$NADP^+$ reductase (FNR, EC 1.18.1.2) (*11*). The FNR family includes the FAD- or FMN-containing domains of over 20 enzymes (*12*) including cytochrome P450 reductase (P450R, EC 1.6.2.4) (*13*), assimilatory nitrate reductase (NR, EC 1.7.1.1) (*14*), nitric oxide synthase (NOS, EC 1.14.13.39) (*15*), and many others. Members of the FNR family provide a valuable model system in which to examine factors regulating pyridine dinucleotide specificity, since within the family there exist both NADP(H)- and NAD(H)-specific enzymes together with bispecific variants. Using site-directed mutagenesis, Shiraishi et al. (*16*) showed that serine 920 and arginine 932 of *N. crassa* NR were critical to the enzyme's ability to discriminate between NADPH and NADH, and that substitution of those residues with aspartate and serine, respectively, allowed for a reversion in specificity. Elmore and Porter focused on the same conserved serine residue (S596) in their examination of CPR NADPH specificity, showing that substitution with an aspartate yielded a NADH-specific enzyme (*17*). Medina et al. probed the contribution to $NAD(P)^+$ selectivity of five residues in *Anabaena* FNR and found that substitution of the same conserved serine residue (S223) with aspartate yielded an appreciable increase in NAD(H) specificity (*18*). On the basis of those observations of NADP(H)-specific FNR family enzymes, the residues believed to confer NAD(P) specificity on several other FNR enzymes have been identified and are shown in the multiple sequence alignment shown in Figure 1. In addition, the primary structures of several recently identified endogenous mammalian cytochrome b_5/cytochrome b_5 reductase fusion proteins (*19*, *20*), which have a preference for NADPH as the electron donor, contain a serine (S422) and an arginine (R437) at the positions believed to regulate coenzyme specificity. To examine whether enhanced specificity for 2′ phosphorylated substrates could be achieved in a NADH-specific member of the FNR family, we have constructed a series of single and double mutants of the soluble diaphorase domain of rat cytochrome b_5 reductase substituted at the residues aspartate 239 and phenylalanine 251 and characterized their utilization of both NADH and NADPH.

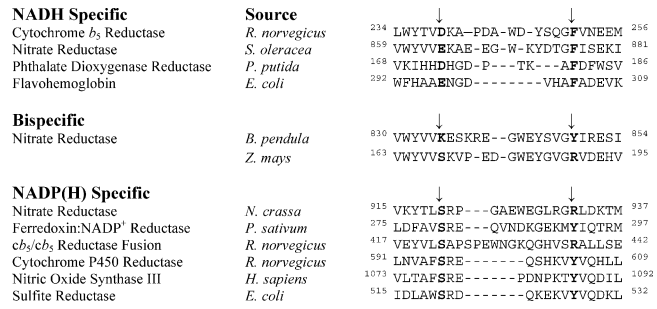

FIGURE 1: Multiple sequence alignment of FNR family enzymes by pyridine nucleotide specificity. Primary sequences of representative members of the FNR family of flavoprotein transhydrogenases that exhibited enhanced specificity for either NAD^+/NADH or $NADP^+$/NADPH were aligned for optimum similarity using the ClustalX algorithm (*39*) together with examples of family members that have been shown to be bispecific. For each sequence, only the residues immediately surrounding the amino acids that have been proposed to regulate nucleotide specificity are shown. The residue positions within the primary sequences are indicated by the superscripts while the arrows indicate residues that have been proposed to be critical in differentiating between hydroxyl and phosphoryl character at the 2′ position of the coenzyme. All sequences were retrieved from GenBank and correspond to NP_620232 (*40*), P23312 (*41*), Q05182 (*42*), S15992 (*43*), RDBJNH (*44*), P39871 (*45*), P08619 (*46*), 1QG0A (*47*), NP_596918 (*20*), P00388 (48), P29474 (49), and P38038 (*50*) accession numbers with respect to the order in which they are listed in the figure.

MATERIALS AND METHODS

Materials. Oligonucleotide primers were obtained from Integrated DNA Technologies (Coralville, IA). *Pfu* Turbo Polymerase as well as *Epicurian coli* BL21(DE3)-RIL cells were obtained from Stratagene (La Jolla, CA). Restriction enzymes were purchased from New England Biolabs (Beverly, MA). Triton X-100 and Hot Start Micro 50 PCR tubes were obtained from Molecular-Bio Products Inc. (San Diego, CA). Tryptone and yeast extract were obtained from EM Science (Gibbstown, NJ). IPTG was obtained from RPI (Mt. Prospect, IL). Reagents for bacterial culture, protein purification, and chemical assays including NADH, NAD^+, NADPH, $NADP^+$, ADP-ribose, ADP, 2′5′-ADP, riboflavin, FAD, $K_3Fe(CN)_6$, and glucose oxidase (*A. niger*) were obtained from Sigma Chemical Co. (St. Louis, MO). Ni-NTA agarose and kits for plasmid preparation and agarose gel extraction were purchased from Qiagen Inc. (Valencia, CA). Nucleotide sequencing was performed by the Molecular Biology Core Facility at the H. Lee Moffitt Cancer Center and Research Institute.

Site-Directed Mutagenesis. CB5R mutants were constructed using whole vector PCR as described previously (*7*) whereby the pH_4CB5R expression construct was specifically mutagenized using complimentary oligonucleotide primers (30−35 mers) with the following sequences: 5′-ctc tgg tac aca gtg **gaa** aaa gc*g* ccc gat gcc tgg g-3′ (D239E), 5′-ctc tgg tac aca gtg **agc** aaa gc*g* ccc gat gcc tgg g-3′ (D239S), 5′-ctc tgg tac aca gtg **acc** aaa gc*g* ccc gat gcc tgg g-3′ (D239T), 5′-tat agc caa ggc **tac** gt*t* aat gag gag atg atc agg-3′ (F251Y), and 5′-tat agc caa ggc **cgc** gt*t* aat gag gag atg atc agg-3′

(F251R), where missense mutations are indicated in bold type and silent mutations are italicized. Silent mutations added a *Hha*I site to the D239 mutant constructs and a *Mse*I site to the F251 mutant constructs for rapid screening. The fidelity of the mutant constructs was verified by nucleotide sequencing in both the forward and reverse directions. Positive constructs were then used to transform competent *E. coli* BL21(DE3)-RIL cells.

Cell Culture and Protein Purification. E. coli BL21(DE3)-RIL cells harboring the pH_4CB5R or mutant constructs were grown aerobically in TB media supplemented with riboflavin (100 μM) overnight at 37 °C. Recombinant protein expression and purification were carried out as described previously (*7*). Wild-type and mutant CB5R concentrations were estimated spectrophotometrically using $A_{461} = 10.6$ cm^{-1} mM^{-1}. SDS−polyacrylamide gel electrophoresis was performed as described by Laemmli (*21*).

Spectroscopy. All spectroscopic measurements utilized oxidized enzymes in 10 mM potassium phosphate buffer, containing 0.1 mM EDTA, pH 7.0. UV/visible spectra were obtained using a Hewlett-Packard (Agilent Technologies, Palo Alto, CA) 8453 diode-array spectrophotometer. UV and visible CD spectra were obtained using a JASCO (Easton, MD) J710 spectropolarimeter, as described previously (*22*). All spectra were corrected for the appropriate buffer contributions and are expressed in terms of molar ellipticities (M^{-1} cm^{-1}). MALDI-TOF mass spectrometric analyses were performed as previously described (*7*).

Enzyme Activities. NAD(P)H:FR activities were determined at 25 °C under conditions of constant ionic strength and pH as previously described (*7*) in 116 mM MOPS buffer, containing 0.1 mM EDTA, pH 7.0 ($\mu = 0.05$). Initial rate data were analyzed using the software "ENZFIT" (Elsevier Biosoft, Ferguson, MO) to yield apparent k_{cat} and K_m values. Specificity ratios were calculated as $(k_{cat}^{NADPH}/K_m^{NADPH})/(k_{cat}^{NADH}/K_m^{NADH})$ where values greater than unity indicate NADPH-specific enzymes and values less than unity represent NADH-specific enzymes.

Charge-Transfer Complex Formation. Reductive titrations were performed under anaerobic conditions as described by Foust (*23*). Enzyme samples (50 μM FAD) in 116 mM MOPS buffer, containing 0.1 mM EDTA, pH 7.0, and NAD(P)H solutions (100 mM) were prepared by repeated evacuation and flushing with O_2-free argon. Enzyme samples were titrated with NADH or NADPH and monitored for increased absorbance in the wavelength range from 600 to 900 nm. Titrations were determined to be saturating when the absorbance at 800 nm ceased to increase and no further bleaching of the flavin spectra occurred following NAD(P)H addition.

Differential Spectroscopy. Spectral binding constants, K_s, for various $NAD(P)^+$ analogues were determined by differential spectroscopic titrations for each of the variants as previously described by Sancho and Gomez-Moreno (*24*) and Barber et al. (*25*). Tetrahydronicotinamide adenine dinucleotides H_4NAD and H_4NADP were synthesized according to the protocol described by Murataliev et al. (*26*). NAD^+, $NADP^+$, 5′-ADP, 2′5′-ADP, H_4NAD, and H_4NADP concentrations were estimated spectrophotometrically. Absorbance changes were plotted versus nucleotide concentration, and a simple hyperbolic equation was used to fit the data and to determine the spectral binding constants.

Stopped-Flow Kinetic Analysis. Rapid-reaction studies of wild-type and the various mutant forms of CB5R with NADH and NADPH were performed using a KinTek SF2002 stopped-flow spectrophotometer (KinTek Corporation, Clarence, PA) thermostated at 7 °C. Experiments were performed using the method described for porcine CB5R by Kimura et al. (*27*) that involved turnover in the presence of both NAD(P)H and ferricyanide. Under these experimental conditions, the initial reaction corresponded to a turnover phase that was followed by a reduction phase when all the ferricyanide had been depleted. Equal volumes of enzyme (50 μM FAD) in 116 mM MOPS buffer, containing 0.1 mM EDTA, pH 7.0, in the presence of 500 μM ferricyanide and varying concentrations of either NADH or NADPH (0.6−4 mM) in 116 mM MOPS buffer, containing 0.1 mM EDTA, pH 7.0, were rapidly mixed and the absorbance of the mixture monitored at 460 and 800 nm wavelengths, respectively. Prior to mixing, all samples were made anaerobic, as described in the section Charge-Transfer Complex Formation with the modification that glucose (10 mM) and glucose oxidase (5 units/mL) were added to the solution prior to introduction into the stopped-flow spectrophotometer. Before use, the syringes and the flow system of the stopped-flow instrument were made anaerobic by overnight treatment with a dilute dithionite solution followed by extensive washing with anaerobic buffer.

Following the NADH:ferricyanide reduction turnover phase, the rate constants (k) for both the NADH:flavin reduction phase (460 nm) and the charge-transfer complex formation phase (800 nm) were analyzed by fitting a single-exponential curve to each absorbance transient using the KinTek SF2002 Software (Version 8.1.0).

Oxidation−Reduction Potential Measurements. Standard oxidation−reduction midpoint potentials for the flavin prosthetic group ($E^{\circ\prime}$, $n = 2$) in wild-type CB5R and selected mutants were determined by the dye equilibration method as described by Massey (*28*) using phenosafranine as the redox indicator ($E^{\circ\prime} = -252$ mV). Briefly, visible absorbance spectra of anaerobic mixtures of dye (15 μM) and enzyme (40 μM) in 100 mM phosphate buffer, pH 7.0, and in the presence or absence of $NAD(P)^+$ (2 mM) were monitored during the course of reduction using xanthine (300 μM) and xanthine oxidase (50 nM). Methyl viologen (6 μM) and benzyl viologen (1 μM) were included to facilitate equilibration of the system. Flavin reduction was monitored at 410 nm whereas phenosafranine reduction was monitored at 530 nm over the course of each 6 h redox titration. Flavin midpoint potentials were calculated from the plot of $\log([\text{oxidized}]/[\text{reduced}])_{FAD}$ versus potential, as indicated by the dye, and are given relative to the standard hydrogen electrode. Midpoint potentials are considered accurate to ±5 mV.

Crystallography. Crystals of CB5R were generated by the sitting drop method as described by Bewley et al. (*10*) using a reservoir of 22% monomethylpoly(ethylene glycol) 2000 in 50 mM sodium acetate at pH 4.8 as precipitant. Data collection was carried out as described previously (*10*), using standard techniques. Data were collected on beamline X12B at the National Synchrotron Light Source, Brookhaven National Laboratory, Upton, NY, using a Quantum 4 CCD. A complete data set was collected from a single crystal for D239T. The mutant crystallized in space group $P2_12_12_1$ with

Table 1. X-ray Diffraction Statistics for the D239T Variant of Cytochrome b_5 Reductase and in Complex with NAD^+

	D239T	D239T+NAD^+
Data Collection Statistics		
unit cell dimensions	$a = 68.09$ Å, $b = 68.87$ Å, $c = 78.64$ Å	$a = 68.43$ Å, $b = 70.00$ Å, $c = 79.81$ Å
resolution range (Å)	30.0−2.2	30.0−2.2
no. of reflections	18987	19477
R_{merge} (%)	5.8 (18.2)	8.0 (19.3)
completeness (%)	98.8 (94.5)	97.9 (83.6)
redundancy	4.1 (3.6)	3.2 (2.8)
$I/\sigma I$	17.3 (4.9)	9.6 (3.2)
Data Refinement Statistics		
resolution range (Å)	30.0−2.2	30.0−2.2
R-factor (%)	20.82	21.90
R_{free} (%)	24.87	24.90
no. of reflections in the R_{free} set	1154	1104
no. of protein atoms	2182	2182
no. of FAD atoms	53	53
no. of NAD^+ atoms	0	44
no. of water molecules	154	162
rmsd bond length (Å)	0.012	0.013
rmsd bond angle (deg)	1.8	1.9

unit cell dimensions $a = 68.09$ Å, $b = 68.87$ Å, $c = 78.64$ Å, and $\beta = 104.7°$. D239T contained one molecule in the asymmetric unit and had an estimated solvent content of 55%. The data collection statistics are shown in Table 1. The structure was solved by molecular replacement in Amore using the protein coordinates of rat CB5R (PDB = 1I7P) (*10*). All subsequent refinement steps used the program CNS, and the models were subject to rigid body refinement. A cycle of simulated annealing and individual isotropic temperature refinement was performed prior to map calculation. The model was fitted to the map, and the FAD molecule was built into the density. Subsequent refinement, punctuated by rounds of model building, was performed until the model could not be improved as judged by a reduction in R_{free}. The refinement statistics are summarized in Table 1. D239T in complex with NAD^+ was crystallized under similar conditions to those for the mutant alone, with the exception that NAD^+ was added to the drop to a final concentration of 40 mM prior to crystallization. A complete data set was collected from a single crystal for D239T. The mutant crystallized in spacegroup $P2_12_12_1$ with unit cell dimensions $a = 68.43$ Å, $b = 70.00$ Å, $c = 79.81$ Å, and $\beta = 104.7°$. D239T contained one molecule in the asymmetric unit and had an estimated solvent content of 60%. The structure of the complex was solved and refined as described for the D239T alone. Statistical analysis of each process is summarized in Table 1. Coordinates for D239T alone and in complex with NAD^+ will be deposited in the Protein Data Bank.

RESULTS

Eight variants of the flavin domain of rat cytochrome b_5 reductase, corresponding to the five single mutants D239E, D239S, D239T, F251R, and F251Y and the three double mutants D239S/F251R, D239S/F251Y, and D239T/F251R, were created using a histidine-tagged CB5R expression system through site-directed mutagenesis. The fidelity of the mutant constructs was verified by dideoxy-sequencing in both directions, and the corresponding proteins were recombinantly expressed in BL21(DE3)-RIL cells. All eight mutants were subsequently purified to homogeneity as judged by the apparent single protein bands following SDS−PAGE analysis as shown in Figure 2. All eight CB5R variants were of similar molecular mass to that of the native enzyme. MALDI-TOF analysis revealed the presence of a characteristic peak in the low mass region of the spectrum with a m/z of 792, indicative of the presence of FAD as the sole prosthetic group.

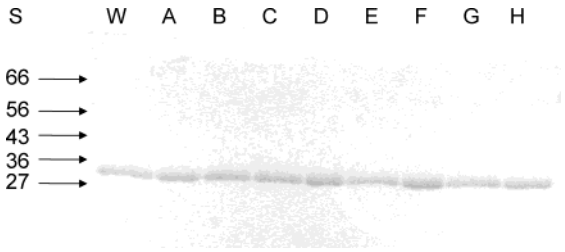

FIGURE 2: SDS−polyacrylamide gel electrophoresis of wild-type and the various mutant forms of cytochrome b_5 reductase. Wild-type CB5R and the various NADPH specificity mutants (2 μg each protein) were isolated as described in the Materials and Methods section and analyzed on a 15% polyacrylamide gel. Lane W, wild-type CB5R; lane A, D239E; lane B, D239S; lane C, D239T; lane D, F251Y; lane E, F251R; lane F, D239S/F251R; lane G, D239S/F251Y; lane H, D239T/F251R. Molecular weight markers (S) are indicated on the left.

UV/visible absorbance spectra were obtained for the wild-type CB5R and each of the single and double mutants. The absorption ratios ($A_{276\ nm}/A_{461\ nm}$) for the mutants varied from 5.5 to 5.9 and were consistent with that of wild-type CB5R (5.5), indicating stoichiometric flavin incorporation. Representative spectra of several of the mutants are shown in Figure 3A and indicate the characteristic absorption maxima at 276, 386, and 461 nm, together with the pronounced shoulder at 485 nm, that are typical of purified CB5R. UV CD spectra were obtained to confirm that neither the single nor double mutations introduced any significant changes in the secondary structural properties of each of the mutants when compared to wild-type CB5R. Representative spectra of several of the mutants, shown in Figure 3B, were nearly identical to those of wild-type CB5R with a positive CD maximum in the range 195−200 nm and a negative CD maximum in the range 215−220 nm, suggesting that none of the substitutions had any deleterious effect on protein folding. In addition, visible CD was used to probe the flavin environment in each of the mutants. Representative spectra, shown in Figure 3C, were very similar to those of wild-type CB5R with positive CD maxima at 310 and 390 nm, respectively, and negative CD maxima at 460 and 485 nm, indicative that the FAD of each mutant was in a similar environment to that of the wild-type CB5R.

Initial-rate kinetic analyses were performed on all eight single and double CB5R mutants to evaluate the effects of the various residue substitutions on NAD(P)H utilization. Values derived for k_{cat} and K_m for both NADH:FR and NADPH:FR activities of the various mutants are given in Table 2 together with the corresponding values for wild-type CB5R. NADH catalytic efficiencies, as indicated by k_{cat}/K_m^{NADH}, were observed to decrease in the order wild-type > F251Y > D239S/F251Y > D239E > F251R > D239S > D239T > D239T/F251R > D239S/F251R with the D239S/F251R variant retaining only 1.1% of the NADH:

Table 2. NAD(P)H:FR Kinetic Constants Obtained for the Wild-Type and Various Mutant Forms of Cytochrome b_5 Reductase

	NADH:FR			NADPH:FR				
enzyme	k_{cat} (s^{-1})	K_m (μM)	k_{cat}/K_m ($s^{-1}\,M^{-1}$)	k_{cat} (s^{-1})	K_m (μM)	k_{cat}/K_m ($s^{-1}\,M^{-1}$)	$\Delta(\Delta G)$[a] kJ mol^{-1}	nucleotide specificity,[b] NADPH/NADH
wild-type	800 ± 21	6.0 ± 1	$1.4 \pm 0.3 \times 10^8$	33 ± 5	924 ± 46	$3.6 \pm 0.8 \times 10^4$	20.4	2.8×10^{-4}
D239E	517 ± 23	6.2 ± 1	$8.6 \pm 1.8 \times 10^7$	5.2 ± 1	94 ± 11	$5.8 \pm 1.8 \times 10^4$	18.3	7.5×10^{-4}
D239S	433 ± 26	17 ± 2	$2.6 \pm 0.5 \times 10^7$	217 ± 14	268 ± 16	$8.2 \pm 1.0 \times 10^5$	8.5	3.4×10^{-2}
D239T	333 ± 18	119 ± 14	$2.87 \pm 0.5 \times 10^6$	267 ± 14	9.1 ± 1	$3.0 \pm 0.2 \times 10^7$	−5.9	1.0×10^1
F251R	500 ± 22	12 ± 2	$4.3 \pm 0.9 \times 10^7$	50 ± 6	138 ± 13	$3.7 \pm 0.8 \times 10^5$	11.8	9.4×10^{-3}
F251Y	367 ± 17	3.1 ± 1	$1.3 \pm 0.5 \times 10^8$	50 ± 8	617 ± 26	$8.1 \pm 1.6 \times 10^4$	18.1	6.6×10^{-4}
D239S/F251R	250 ± 23	224 ± 20	$1.13 \pm 0.2 \times 10^6$	200 ± 12	22 ± 3	$9.3 \pm 1.8 \times 10^6$	−5.2	8.1×10^0
D239S/F251Y	467 ± 21	5.3 ± 1	$9.2 \pm 2.1 \times 10^7$	417 ± 21	25 ± 3	$1.7 \pm 0.3 \times 10^7$	4.3	1.7×10^{-1}
D239T/F251R	717 ± 27	512 ± 42	$1.4 \pm 0.2 \times 10^6$	550 ± 23	44 ± 5	$1.3 \pm 0.2 \times 10^7$	−5.4	8.9×10^0

[a] $\Delta(\Delta G) = -RT \ln[(k_{cat}/K_m^{NADPH})/(k_{cat}/K_m^{NADH})]$, where $T = 298$ K and $R = 8.314$ kJ mol^{-1} K^{-1}. $\Delta(\Delta G)$ is an indication of the difference in binding energy between NADH and NADPH. [b] Nucleotide specificity is calculated as $(k_{cat}/K_m(\text{NADPH}))/(k_{cat}/K_m(\text{NADH}))$.

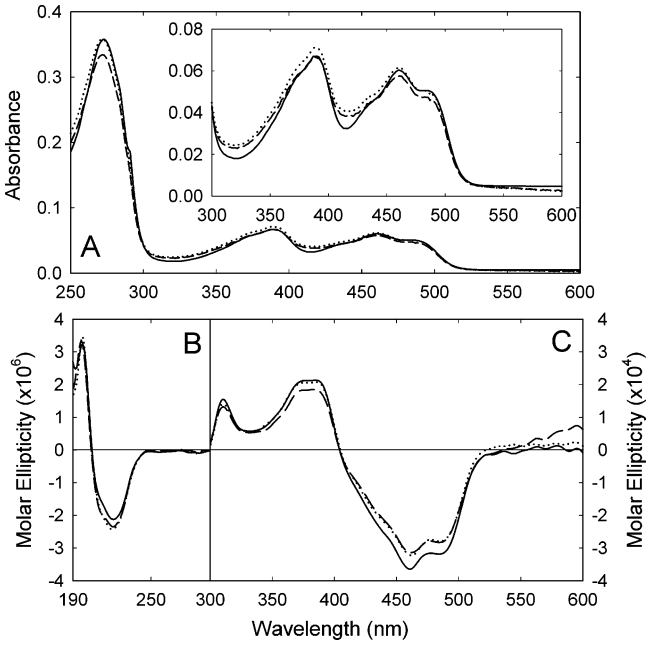

FIGURE 3: UV/visible absorbance and CD spectra of the wild-type and various mutant forms of cytochrome b_5 reductase. Panel A: UV/visible spectra were recorded for oxidized samples of wild-type and mutant forms of CB5R (5 μM FAD) in 10 mM phosphate buffer, containing 0.1 mM EDTA, pH 7.0. Individual absorbance spectra correspond to wild-type (—), D239T (- - -), and D239T/F251R (• • •). Panel B: CD spectra in the far UV (190−250 nm) and near UV (250−300 nm) wavelength range were determined for the wild-type, D239T, and D239T/F251R forms of CB5R (7 μM FAD) in 10 mM phosphate buffer, containing 0.1 mM EDTA, pH 7.0 The line shapes are the same as those in panel A. Panel C: CD spectra in the visible (300−600 nm) wavelength range were determined for wild-type, D239T, and D239T/F251R CB5R (60 μM FAD) in 10 mM phosphate buffer, containing 0.1 mM EDTA, pH 7.0. The line shapes are the same as those in panel A.

FR efficiency of the wild-type protein. In contrast, NADPH:FR efficiencies, as indicated by the values of k_{cat}/K_m^{NADPH}, increased in the order wild-type > D239E > F251Y > F251R > D239S > D239S/F251R > D239T/F251R > D239S/F251Y > D239T with the D239T mutant exhibiting an 823-fold increase in NADPH:FR efficiency when compared to the wild-type protein.

The values for the NAD(P)H specificity constant (defined as the ratio of $\{k_{cat}/K_m^{NADPH}\}/\{k_{cat}/K_m^{NADH}\}$) listed in Table 2 reflect the magnitudes of the individual k_{cat} and K_m values obtained for both NADH and NADPH and were observed to increase in the order wild-type < D239E < F251Y < F251R < D239S < D239S+F251Y < D239S+F251R < D239T+F251R < D239T. As anticipated, conservative substitutions of D239 with glutamate and F251 with tyrosine, respectively, had the least impact on improving CB5R function with NADPH, corresponding to only an approximate 2-fold increase in NADPH:FR activity. In contrast, the D239S/F251Y double mutant showed a 460-fold increase in NADPH catalytic efficiency while retaining 70% of the wild-type NADH catalytic efficiency, indicating the D239S/F251Y represented the most bispecific variant. Each of the remaining double mutants, corresponding to D239S/F251R and D239T/F251R, exhibited improved NADPH efficiency coupled with compromised NADH efficiency. The D239T/F251R variant displayed the desired properties of rapid turnover of NADPH together with a high Michaelis constant for NADH. However, the mutant lacked a low Michaelis constant for NADPH that would be desirable in an efficient NADPH-utilizing form of CB5R. Comparison of the initial-rate kinetic parameters of the CB5R variants constructed in this study revealed that the single mutant, D239T, represented the most efficient NADPH-utilizing variant, exhibiting a 39200-fold preference for NADPH over NADH. Therefore, all additional studies were limited to comparing the properties of D239T and wild-type CB5R.

To further examine the interactions of the wild-type and D239T variants of CB5R with both NADH and NADPH, we monitored the production of the characteristic charge-transfer complex formed between the reduced enzyme and $NAD(P)^+$. Spectroscopic data obtained during reductive titrations of wild-type CB5R with either NADH or NADPH are shown in parts A and B, respectively, of Figure 4 while the results of identical experiments performed with the D239T variant are shown in parts C and D of Figure 4. The observed increase in absorbance in the near-IR region of the spectrum (700−900 nm), concomitant with the associated bleaching of the flavin absorbance in the visible region (400−500 nm), has been attributed to the formation of a stable $FADH^-$:NAD^+ charge-transfer complex (*29*). The titration results illustrated that the wild-type enzyme readily formed a stable charge-transfer complex with NADH but was able to form a charge-transfer complex with NADPH to only a limited extent, even at NADPH concentrations > 1 mM. In contrast, the D239T variant was observed to readily form productive complexes with both NADH and NADPH, indicating a reduction in specificity compared to the case of the wild-type enzyme.

Pre-steady-state kinetic analyses were utilized to compare the rates of hydride ion transfer for both the wild-type and

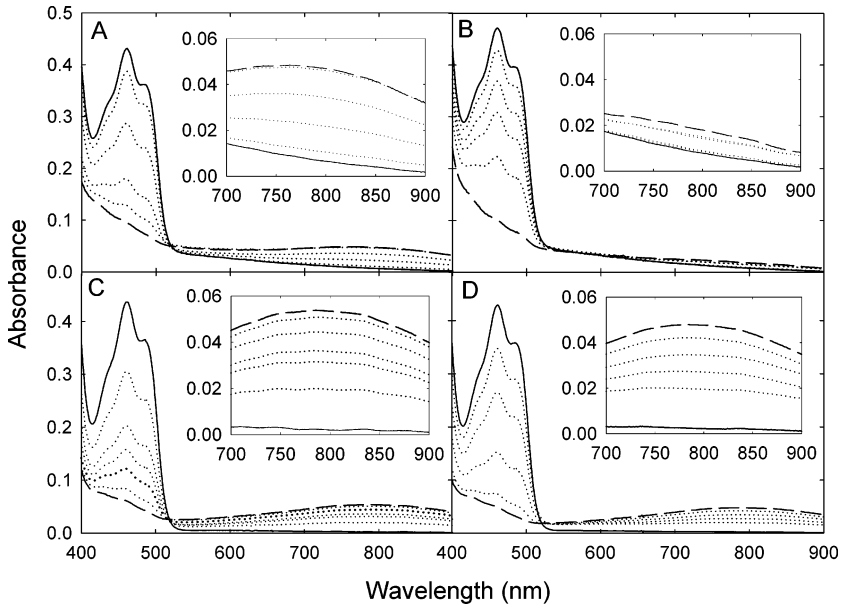

FIGURE 4: Charge-transfer complex formation for the wild-type and D239T variants of cytochrome b_5 reductase with NAD(P)H. Enzyme samples (50 μM FAD) in 116 mM MOPS buffer, containing 0.1 mM EDTA, pH 7.0, were prepared in a sealed cuvette and made anaerobic as described in the Materials and Methods section. Visible/near-IR absorbance spectra were recorded during the enzyme titrations following additions of either NADH or NADPH, respectively. Oxidized spectra (—), intermediate spectra (· · ·), and fully reduced spectra (- - -) are shown. The insets focus on the near-IR region of the spectrum. Panel A: Wild-type + NADH. Panel B: Wild-type + NADPH. Panel C: D239T + NADH. Panel D: D239T + NADPH. Only selected spectra obtained during the titrations are shown for clarity.

D239T variants of CB5R with either NADH or NADPH. Flavin reduction was monitored by the decrease in absorbance at 460 nm while charge-transfer complex formation was monitored by the increase in absorbance at 800 nm. Kinetic transients obtained for the reaction of wild-type CB5R with either 4 mM NADH or 4 mM NADPH are shown in parts A and B, respectively, of Figure 5 while the results of identical experiments performed with the D239T variant are shown in parts C and D of Figure 5. A concentration of 4 mM NAD(P)H was used to approximate saturation, though statistical analysis for determination of actual k_{lim} and K_d values could not be performed due to low signal-to-noise ratios at substrate concentrations below 0.6 mM. The initial phases of the stopped-flow traces indicated the flavin cofactor to be predominantly in the oxidized state during turnover in the presence of excess $NAD(P)^+$ and limiting ferricyanide concentrations, respectively. However, following consumption of the ferricyanide, the kinetic transients reflected reduction and the associated bleaching of the flavin absorbance at 460 nm together with the formation of the $FADH^-$:NAD^+ charge-transfer complex at long wavelengths.

Rate constants derived for the various transients are listed in the legend of Figure 5. Reduction of the wild-type enzyme with either NADH or NADPH and the associated formation of the respective charge-transfer complexes were both observed to be monophasic processes. However, rate constants obtained for flavin reduction and charge-transfer complex formation with NADH were determined to be 20-fold greater than those with NADPH, reflecting the physiological specificity of the wild-type enzyme for the 2′-hydroxylated coenzyme. For the D239T variant, both NADH and NADPH reduction were determined to be more rapid than those for the wild-type enzyme. NADH reduction was increased approximately 1.4-fold while NADPH reduction increased 15-fold. Comparable changes in the rates of charge-transfer complex formation were also observed.

To compare the interactions of the wild-type and D239T variants of CB5R with NAD^+, $NADP^+$, and a variety of pyridine nucleotide analogues, differential spectroscopy was utilized to monitor complex formation. Perturbations of the flavin visible absorbance spectrum, shown in Figure 6, were detected for the wild-type enzyme during titrations with NAD^+, 5′-ADP, and H_4NAD but not with $NADP^+$, 2′5′-ADP, and H_4NADP. In contrast, spectroscopically detectable complexes were observed for the D239T variant and all of the pyridine nucleotide analogues examined. Values derived for the respective spectral binding constants, K_s, for the wild-type and D239T variants of CB5R are listed in the legend of Figure 6. As anticipated, wild-type CB5R was observed to bind NAD^+ with a significantly greater affinity than that for $NADP^+$ whereas the reverse behavior was observed for D239T, which bound $NADP^+$ with a greater affinity than that for NAD^+.

Comparison of the results obtained for binding of 5′-ADP and 2′5′-ADP to both the wild-type enzyme and the D239T variant revealed an alternate pattern of affinities. D239T exhibited a greater affinity for 5′-ADP when compared to wild-type CB5R whereas complex formation with 2′5′-ADP was only detectable for D239T, although with a reduced affinity than that with 5′-ADP. These results suggest that while analogues with 2′-phosphoryl groups are readily accommodated by D239T, additional contacts made with other active site residues may be more critical to achieving the correct orientation of analogue binding. Since 5′-ADP and 2′5′-ADP are smaller molecules and binding requires fewer contacts at the active site, the presence of the phosphate at the 2′ position is more detrimental than it is in the larger analogues. To test this hypothesis, we examined the binding of H_4NAD and H_4NADP (*26*) to both the wild-type enzyme and the D239T variant. These tetrahydronicotinamide derivatives do not function as hydride donors when substituted for NADH in either the NADH:FR or NADH:BR CB5R assays

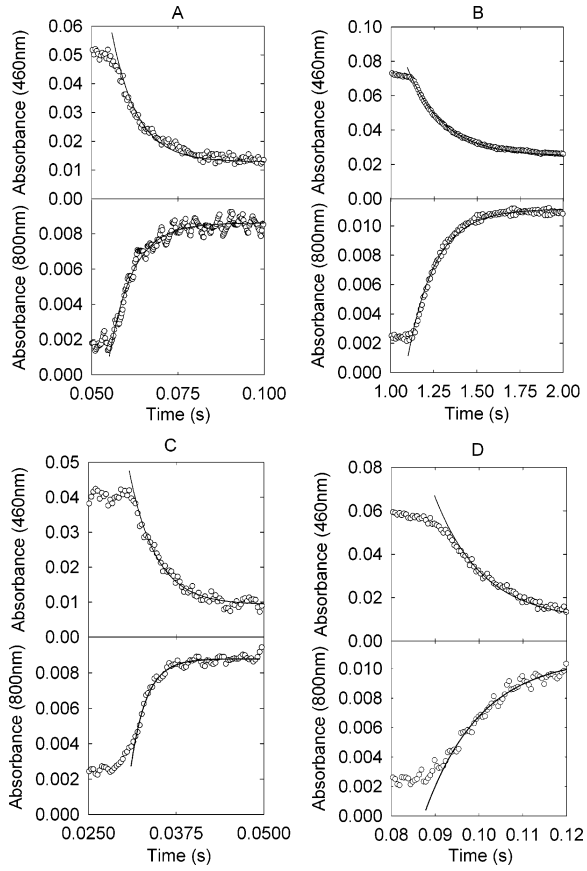

FIGURE 5: Stopped-flow kinetic transients of flavin reduction using NAD(P)H of wild-type and D239T cytochrome b_5 reductase. Enzyme samples (50 μM FAD) in 116 mM MOPS buffer, containing 0.1 mM EDTA and 500 μM ferricyanide, pH 7.0, and solutions of NAD(P)H (4 mM) were made anaerobic as described under the Materials and Methods section and rapidly mixed in the stopped-flow apparatus at 7 °C. Panels A and B: Wild-type CB5R reduced with NADH and NADPH, respectively. Panels C and D: D239T reduced with NADH and NADPH, respectively. In each panel, the upper transient monitors flavin reduction at 460 nm, while the lower transient corresponds to the formation of the charge-transfer complex, detected at 800 nm. Individual data points are shown (○) while the solid line corresponds to the single-exponential fit of the data. The rate constants for hydride ion transfer were $k^{WT-NADH} = 130 \pm 12\ s^{-1}$ and $k^{WT-NADPH} = 5 \pm 1\ s^{-1}$ for wild-type CB5R while the corresponding values for the D239T variant were $k^{D239T-NADH} = 180 \pm 17\ s^{-1}$ and $k^{D239T-NADPH} = 73 \pm 5\ s^{-1}$. The rate constants for charge-transfer complex formation were $k^{WT-NADH} = 150 \pm 20\ s^{-1}$ and $k^{WT-NADPH} = 7 \pm 1\ s^{-1}$ for wild-type CB5R while the corresponding values for the D239T variant were $k^{D239T-NADH} = 210 \pm 28\ s^{-1}$ and $k^{D239T-NADPH} = 70 \pm 3\ s^{-1}$.

but are valuable tools for examining the binding affinity for NADH and NADPH, respectively. Both H_4-nucleotides are close isosteric analogues and are assumed to involve the same contacts at the active site as NADH or NADPH, but they lack the positive charge on the nicotinamide ring that is present on NAD^+ and $NADP^+$. The binding of H_4NAD produced a completely different perturbation of the wild-type CB5R visible spectrum than NAD^+, indicating that the charge on the nicotinamide ring influenced nucleotide binding in CB5R. H_4NAD bound with higher affinity to wild-type CB5R than any other analogue examined and, as anticipated, bound with lower affinity to the D239T variant. H_4NADP produced a similar perturbation in the spectrum of D239T and bound with an affinity comparable to that of H_4NAD. Comparison of the K_s values obtained for the binding of H_4NAD and H_4NADP to D239T with those obtained for the binding of 5′-ADP and 2′5′-ADP confirmed that a 2′ phosphate was more easily accommodated at the active site when a greater number of contacts was made with the pyridine nucleotide. The observation that wild-type CB5R was unable to bind any of the 2′ phosphorylated analogues suggests an important role for D239 in differentiating between NADH and NADPH.

To examine whether substitution of D239 influenced NADPH utilization through modulation of the flavin midpoint potential, redox titrations were performed using the dye equilibration method for wild-type CB5R and the D239T variant in the presence of phenosafranine ($E^{\circ\prime} = -252$ mV). Flavin midpoint potentials ($E^{\circ\prime}$, $n = 2$) were determined for the enzymes alone and in complex with NAD^+ and $NADP^+$, respectively. Representative spectra obtained during the course of the titrations are shown in Figure 7A for wild-type CB5R and in Figure 7B for the D239T variant. Qualitative analysis of the individual spectra indicated that the majority of the phenosafranine was reduced prior to FAD reduction for both enzymes in the absence of any pyridine nucleotide, suggesting the flavin midpoint potentials were more negative than that of phenosafranine, for either enzyme alone. In contrast, analysis of the spectra for each enzyme in the presence of NAD^+ revealed that the majority of the flavin was reduced prior to the dye, suggesting that both complexes had more positive flavin midpoint potentials than phenosafranine. In the presence of $NADP^+$, the flavin of wild-type CB5R and the phenosafranine were reduced simultaneously, indicating approximately equivalent midpoint potentials. However, the flavin of D239T in the presence of $NADP^+$ was reduced prior to the dye, indicating a more positive midpoint potential. In the long wavelength range from 600 to 1000 nm, charge-transfer species were again detectable for both enzymes in complex with NAD^+, for D239T in complex with $NADP^+$, and to a lesser extent for the wild-type CB5R−$NADP^+$ complex.

The flavin redox potentials ($n = 2$) for each enzyme and enzyme−nucleotide complex were determined from Nernst semilog plots as shown in Figure 7C. The standard midpoint potentials obtained for the FAD/$FADH_2$ couple in both the wild-type enzyme ($E^{\circ\prime} = -268$ mV) and the D239T variant ($E^{\circ\prime} = -272$ mV) were approximately equivalent for both proteins in the absence of any pyridine nucleotide, with the values differing by only 4 mV. In contrast, significant differences in flavin midpoint potential were observed for the wild-type CB5R and the D239T variant in the presence of either NAD^+ or $NADP^+$. In the presence of NAD^+, the redox potential of the FAD/$FADH_2$ couple in the wild-type enzyme was positively shifted by 78 mV ($E^{\circ\prime} = -190$ mV) whereas, in the presence of $NADP^+$, a substantially smaller positive perturbation of only 15 mV was observed ($E^{\circ\prime} = -253$ mV). However, for the D239T variant of CB5R, comparable positive shifts, of the order of 60−70 mV, were observed in the presence of either NAD^+ or $NADP^+$, yielding potentials of −206 mV for the FAD/$FADH_2$ couple in the D239T−NAD^+ complex and −215 mV in the D239T−$NADP^+$ complex, respectively.

To examine the changes in the structure of the D239T variant at the atomic level, crystallographic studies were performed to define the specific structural alterations responsible for the observed switch of pyridine nucleotide

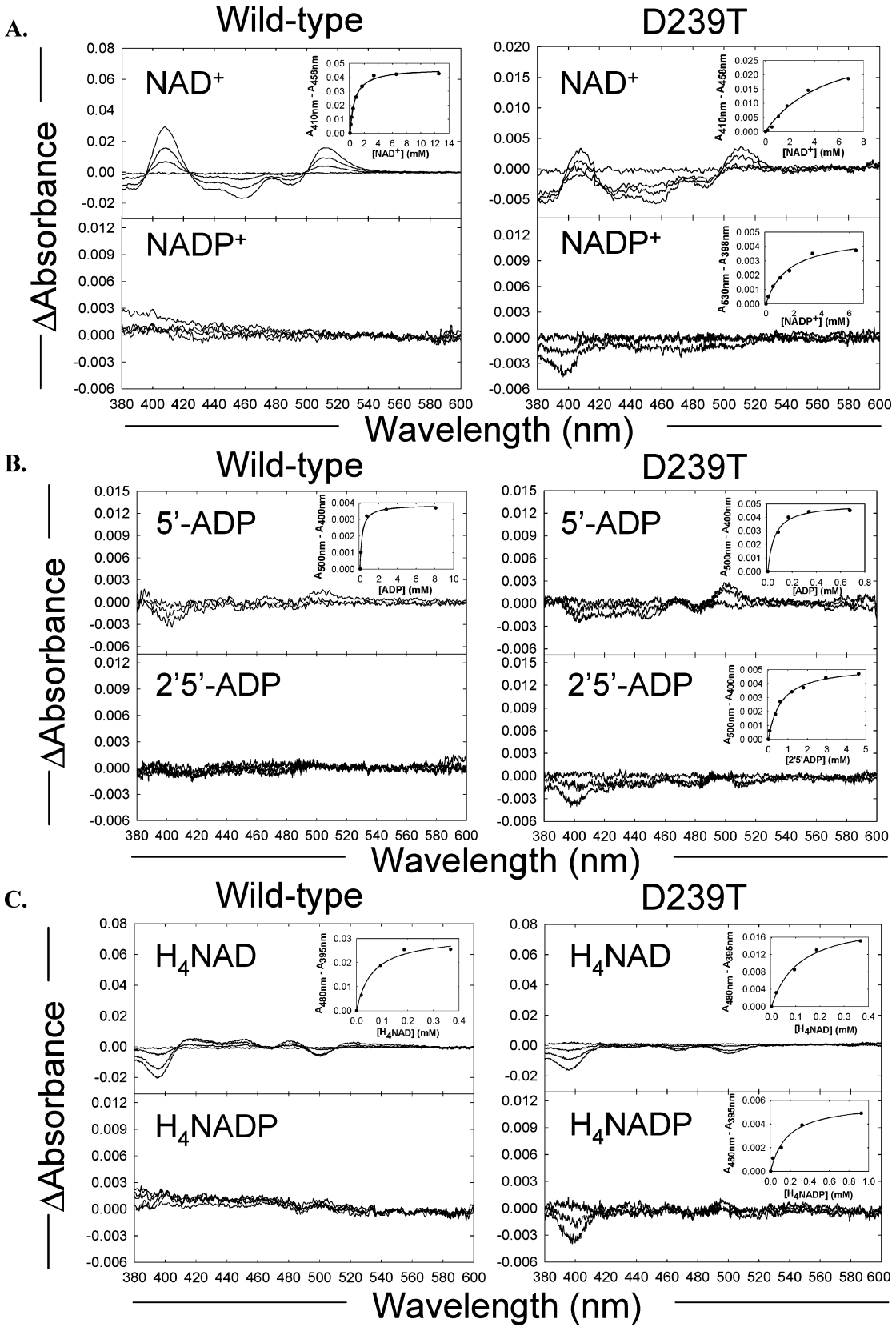

FIGURE 6: Difference spectra and spectral binding constant determinations for wild-type and D239T cytochrome b_5 reductase with various pyridine nucleotide analogues. Enzyme samples (50 μM FAD) in 20 mM MOPS buffer, containing 0.1 mM EDTA, pH 7.0, were titrated with the indicated pyridine nucleotides as described under the Materials and Methods section. The difference spectra obtained during the titrations of wild-type (left panels) and D239T (right panels) with NAD(P)$^+$ (panel A), 2′5′-ADP (panel B), and H_4NAD(P) (panel C) are shown. Where a difference spectrum was detected, the inset panel corresponds to a plot of the spectral perturbations (peak to trough measurements at the indicated wavelengths) versus pyridine nucleotide concentration. K_s values obtained for the wild-type enzyme were $K_s^{NAD^+} = 760 \pm 30$ μM, $K_s^{5'ADP} = 100 \pm 20$ μM, and $K_s^{H_4NAD} = 45 \pm 10$ μM, while values for NADP$^+$, 2′5′-ADP, and H_4NADP were not determined. K_s values obtained for the D239T variant were $K_s^{NAD^+} > 5000$ μM, $K_s^{NADP^+} = 1600 \pm 250$ μM, $K_s^{5'ADP} = 55 \pm 10$ μM, $K_s^{2'5'ADP} = 600 \pm 150$ μM, $K_s^{H_4NAD} = 115 \pm 20$ μM, and $K_s^{H_4NADP} = 170 \pm 50$ μM.

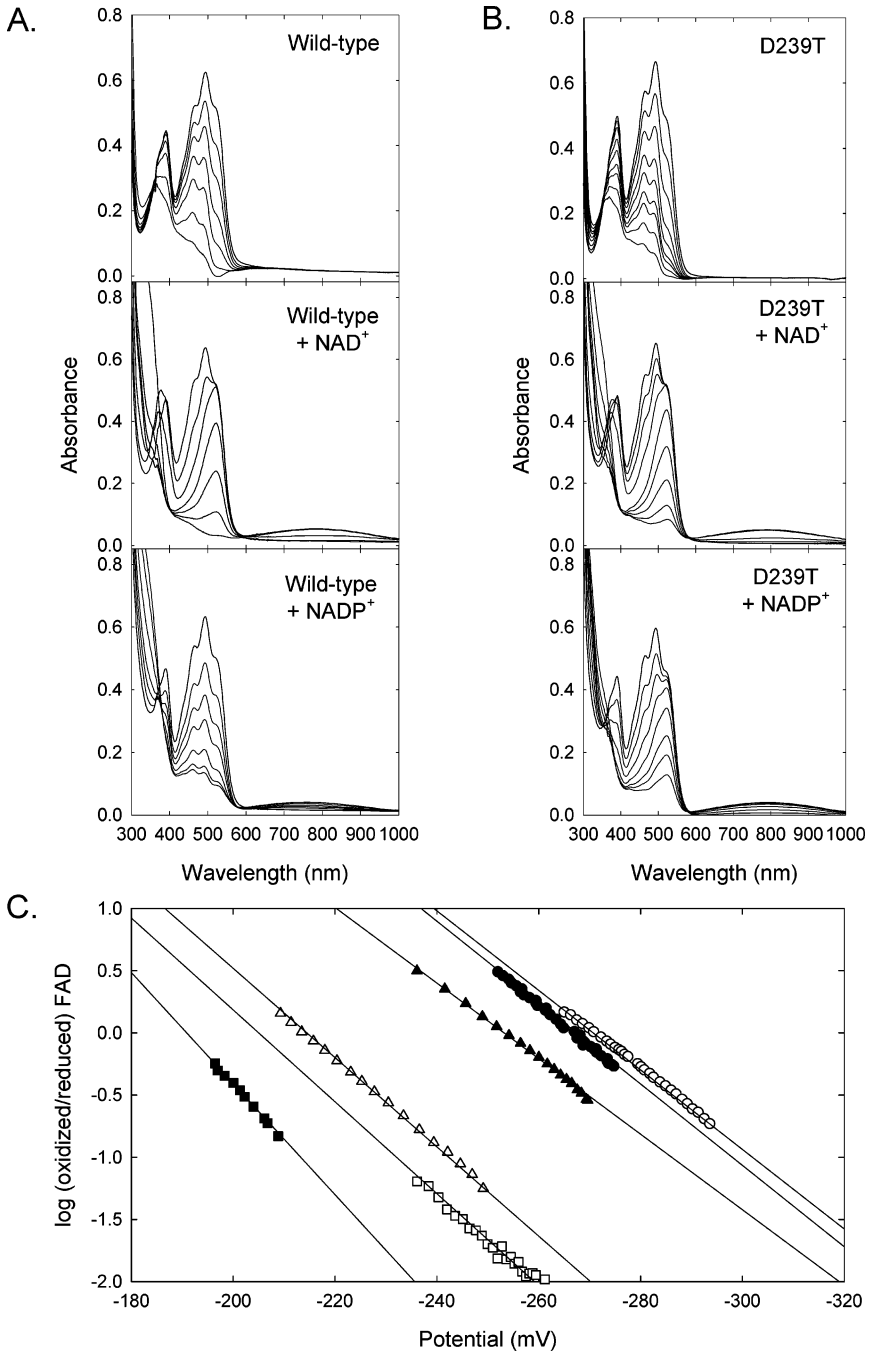

FIGURE 7: Oxidation−reduction midpoint potential determinations for the flavin cofactor in wild-type cytochrome b_5 reductase and the D239T variant. Reductive dye equilibration titrations of wild-type CB5R (panel A) and the D239T (panel B) variant (40 μM FAD each enzyme) were performed as described under the Materials and Methods section in the absence and presence of either NAD^+ or $NADP^+$ (2 mM), respectively, in 100 mM phosphate buffer, containing 0.1 mM EDTA, pH 7.0, in the presence of phenosafranine (15 μM, $E^{o\prime} = -252$ mV) (*28*). Individual spectra were collected at 2−3 min intervals during the time course of the titrations, and selected spectra are shown in panels A and B. The corresponding Nernst plots are shown in panel C and correspond to wild-type CB5R alone (●, $E^{o\prime} = -268$ mV), D239T alone (○, $E^{o\prime} = -272$ mV), wild-type CB5R+NAD^+ (■, $E^{o\prime} = -190$ mV), D239T+NAD^+ (□, $E^{o\prime} = -206$ mV), wild-type CB5R+$NADP^+$ (▲, $E^{o\prime} = -253$ mV), and D239T+$NADP^+$ (△, $E^{o\prime} = -215$ mV), respectively.

specificity. The structures of the oxidized D239T mutant in both the absence and presence of NAD^+ were determined each to a resolution of 2.2 Å. The structure of D239T is shown in Figure 8 and exhibits the same fold as that of the wild-type protein (PDB = 1I7P) (*10*), as shown by the low root-mean-square deviations (rms deviation 0.58 Å) of the C_α backbone, indicating little difference in the position of the main-chain carbon atoms and indicating identical secondary and tertiary structural features (Figure 8A) in the mutant. The FAD cofactor also aligned well in each of the structures (rms deviation 0.52 Å). While no changes in the C_α backbone at the mutated position were observed, the major change between the wild-type structure and that of the D239T variant in this region was a decrease in the lengths of the two parallel β-strands that comprise residues V202−S211 and F232−K240. This is a consequence of the fact that strand 2 is strongly stabilized by the adjacent strand 3 of the β-sheet. The structural changes in the D239T variant can be explained by the alterations in the H-bonding network in this region of the structure following the mutation.

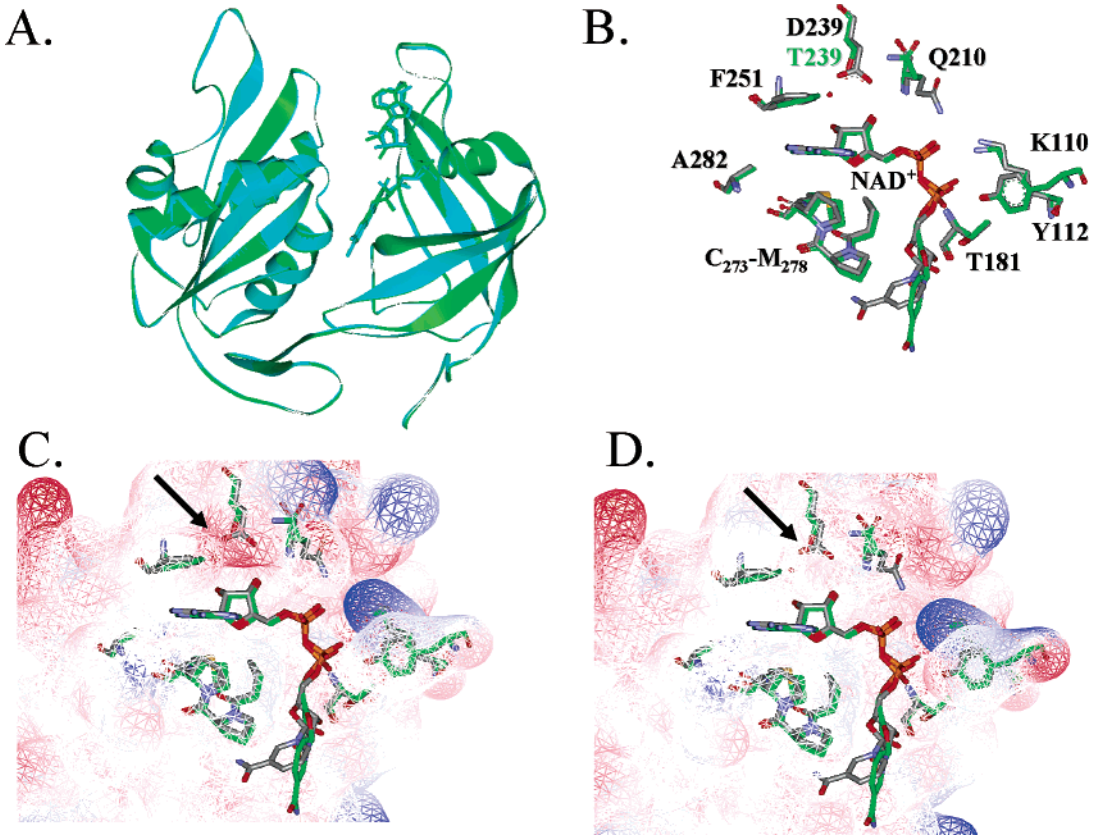

FIGURE 8: Structure of the D239T cytochrome b_5 reductase variant at 2.2 Å resolution, and in complex with NAD^+ at 2.2 Å resolution. The structure of D239T was determined as described under the Materials and Methods section. Panel A: The structures of wild-type CB5R (cyan ribbon), reported previously (*10*), and D239T (green ribbon) are superimposed to show identical global folding of the two enzymes. Panel B: The structures of wild-type CB5R in complex with NAD^+ (shown as CPK sticks), also reported previously (*10*), and D239T in complex with NAD^+ (CPK sticks with carbons colored green) are superimposed. Residues that form contacts with the ADP portion of the NAD^+ molecule are labeled. "*" denotes the altered position of the side chain atoms of glutamine 210 in the D239T structure. Panel C: The same structures, displayed using the same configuration as that in panel B, have the electrostatic surface of the wild-type NAD^+−ADP binding site represented as a mesh with positively charged regions colored in blue and negatively charged regions colored in red, respectively. The arrow indicates the surface created by the side chain atoms of D239. Panel D: The electrostatic surface of the wild-type protein has been replaced with that of the D239T mutant. The arrow indicates the loss of the negatively charged surface attributable to D239 when substituted with the polar uncharged threonine residue.

Comparison of the structures of the D239T mutant alone and in complex with NAD^+ revealed no significant alterations in the fold (rms deviation 0.35 Å for all C_α). In the structure of the D239T−NAD^+ complex, the ADP moiety of the pyridine nucleotide was clearly resolved and, with the exception of the 2′-OH group, made the same contacts previously identified in the wild-type CB5R−NAD^+ complex (Figure 8B). The primary structural difference involved the positions of the side chain atoms of residues Q210 and D239. In wild-type CB5R, the side chain of residue D239 was solvent exposed and formed the negatively charged surface for 2′-OH binding. In the D239T mutant, the side chain of residue T239 was directed away from the NAD^+, leaving only the side chain O_γ exposed at the binding surface, which superimposed onto the position of the Cγ in the wild-type structure. This placed the T239 O_γ atom 4.6 Å from the NAD^+ 2′-OH in the structure of the mutant, whereas the side chain oxygen atoms of D239 were within hydrogen bonding distance of the 2′-OH and 3′-OH oxygen atoms of the FAD in the wild-type CB5R structure. In addition, the side chain atoms of Q210 were displaced away from the pyridine binding cleft in the D239T−NAD^+ complex structure. However, in contrast to the case of the wild-type−NAD^+ complex, the position of the nicotinamide moiety in the D239T−NAD^+ complex was observed in an altered conformation that resulted from a rotation around the ribose−nicotinamide linkage. In this conformation, the nicotinamide ring was closer to the flavin isoalloxazine ring, although the C4 was still over 10 Å away from the N5 atom of the isoalloxazine ring, a distance incompatible for efficient hydride transfer.

DISCUSSION

This study represents the first examination of the roles of specific amino acid side chains in regulating the coenzyme specificity of cytochrome b_5 reductase. We have applied rational protein engineering principles to alter the pyridine nucleotide specificity of CB5R from the physiological preference for the electron donor, NADH, to the preference for the 2′-phosphorylated form, NADPH. Our mutagenic strategy was based on previous studies of NAD(P)H binding determinants in the FNR family of flavoproteins (*16*−*18*) and on the previously published structure for rat CB5R (*10*).

Eight variants of CB5R were produced, including five single and three double mutants, all of which were purified to homogeneity and determined to contain stoichiometric levels of FAD. Of the eight mutants created, three were determined to be NADPH-specific, one was NAD(P)H

bispecific, and the remaining four were NADH-specific, on the basis of measurements of their respective NADH:FR and NADPH:FR activities. Wild-type CB5R had a 3700-fold preference for NADH over NADPH whereas the D239T variant, which corresponded to the most NADPH-specific variant of those engineered, had an approximate 11-fold preference for NADPH versus NADH. This change represented a 39200-fold increase in NADPH specificity. To attain the same level of specificity observed for NADH by wild-type CB5R, a (1.3×10^6)-fold increase in the preference for NADPH would have been required. Thus, the results suggest that, despite the observed 11-fold preference for NADPH over NADH exhibited by the D239T variant, this mutant should more accurately be classified as bispecific.

To understand how substitution of a single residue facilitated the switch of coenzyme specificity, the D239T mutant was analyzed kinetically, thermodynamically, and structurally. Anaerobic titrations of both wild-type and D239T CB5R variants with either NADH or NADPH confirmed that the wild-type enzyme did not utilize NADPH efficiently. In contrast, D239T formed stable charge-transfer complexes with both coenzymes, providing further evidence of its bispecific identity. Similar conclusions were evident following the stopped-flow analyses of each of the enzymes. The rate of hydride ion transfer was rapid for wild-type CB5R with NADH and slow with NADPH whereas the D239T variant showed a small preference for NADH compared to NADPH, a trend that is in agreement with the steady-state data only if product release and inhibition are considered in the catalytic mechanism. To address the possibility of the roles of product release in the kinetic mechanism, spectroscopic binding constants (K_s) were determined for various 2′-hydroxylated and 2′-phosphorylated nucleotides. These studies confirmed that wild-type CB5R did not bind nucleotides with a phosphate group at the 2′ position. However, the D239T mutant had a relatively high affinity for $NADP^+$ compared to NAD^+, suggesting that, under the conditions used in the stopped-flow studies which involved production of significant levels of the oxidized nucleotides, $NADP^+$ inhibition or $NADP^+$ product release may have complicated the analysis of the NADPH reaction with the enzyme. Differential spectroscopy also revealed that the tetrahydropyridine nucleotides were better mimics of NADH compared to NAD^+ due to the absence of the positive charge on the nicotinamide ring.

The values obtained for the $FAD/FADH_2$ redox couple in both wild-type CB5R and the D239T variant indicated that substitution of a threonine residue for the aspartic acid side chain at position 239 had no significant effect on the thermodynamic properties of the flavin prosthetic group. For the wild-type CB5R, the flavin midpoint potential ($E^{\circ\prime} = -268$ mV) was in very good agreement with the value of −258 mV previously reported by Iyanagi (*30*) for the porcine enzyme, which was determined by dithionite titration in the presence of indigodisulfonate and safranine T as mediators.

In contrast to the results obtained for the potentiometric titrations of the wild-type and D239T forms of CB5R alone, significant differences in flavin redox potential were detected between the two proteins in the presence of either NAD^+ or $NADP^+$. For the wild-type CB5R, complex formation with NAD^+ was observed to result in a significant positive shift of the $FAD/FADH_2$ redox couple, which reflected the greater affinity for the NAD^+ of the reduced form compared to the oxidized form of the enzyme. A similar shift in flavin potential has previously been reported for the porcine CB5R following titrations with NADH (*30*) or dithionite in the presence of NAD^+ (*31*). As anticipated, complex formation of wild-type CB5R with $NADP^+$ resulted in a positive shift in the flavin redox potential, although of substantially smaller magnitude, due to the lower affinity of the enzyme for the nonphysiological form of the substrate. However, for the D239T variant, significant positive shifts in the flavin redox potential were observed in the presence of either NAD^+ or $NADP^+$, confirming the bispecific identity of the mutant and suggesting that coenzyme binding is important in modulating the thermodynamic properties of the flavin prosthetic group of CB5R during turnover (*31*).

The crystal structures of D239T and the D239T−NAD^+ complex clearly illustrated that replacement of aspartate 239 with threonine abolished the negative electrostatic character of the coenzyme binding surface near the 2′ position of the ADP moiety. This change occurred in concert with two other transitions: the displacement of the side chain atoms of lysine 240 away from the coenzyme binding site and the movement of the side chain atoms of glutamine 210. The overall effect was to abolish both the steric hindrance and charge repulsion that precluded 2′-phosphate binding in the wild-type enzyme. Superposition of NADPH from the crystal structure of ferredoxin:$NADP^+$ reductase (*32*) indicated that the 2′ phosphate group was able to be accommodated in the D239T structure without any steric clashes. Further, the position of the side chain nitrogen atom of Q210 would be within hydrogen-bonding distance of one of the phosphate oxygen atoms, suggesting that the D239T not only obliterates steric and charge incompatibilities but also begins to shape a binding site for the 2′-phosphate group.

On the basis of these results, aspartate 239 represents a key determinant of coenzyme specificity in CB5R, in good agreement with the results of pyridine nucleotide specificity studies of the corresponding residue in other members of the FNR family. Replacement of aspartate 239 with threonine significantly enhanced the NADPH specificity of CB5R. However, attempts to further enhance the specificity of CB5R toward NADPH will potentially require the creation of a positive charge on the surface of the newly created 2′ phosphate binding cleft, not at position 251 but more likely at position 210.

The capacity to rapidly generate a diverse array of recombinant proteins has made it possible to engineer redox enzymes with altered substrate specificities. As the use of redox enzymes in combination with the chemical catalysts that are currently used in the industrial and pharmaceutical synthesis of compounds increases, the ability to engineer their function will become invaluable (*33*). For pyridine nucleotide-utilizing enzymes, considerable effort has been applied to altering coenzyme specificity with mixed results. Attempts to alter either the NAD^+/NADH or $NADP^+$/NADPH specificity of a variety of reductases/dehydrogenases have been previously reported from both prokaryotic and eukaryotic sources, as shown in Table 3. The results of these alteration studies, which have been equally divided between both NAD^+/NADH- and $NADP^+$/NADPH-utilizing enzymes, have varied from a from a high of a (2.5×10^6)-fold change in $NADP^+$ utilization by *S. cerevisiae* formate dehydrogenase

Table 3. Summary of the Results of Various Enzyme NAD(P)(H) Specificity Engineering Studies

enzyme	source	specificity	mutation(s)	improvement[a]	ref
cytochrome b_5 reductase	*R. norvegicus*	NADH → NADPH	D239T	39200	
nitrate reductase	*S. oleracea*	NADH → NADPH	E864S+F876R	6150	38
malate dehydrogenase	*T. flavus*	NADH → NADPH	E41-K47 loop	132	51
lactate dehydrogenase	*B. stearothermophilus*	NADH → NADPH	I51K+D52S	55	52
glyceraldehyde-3-phosphate dehydrogenase	*B. stearothermophilus*	NAD^+ → $NADP^+$	D32A+L187A+P188S	NA	53
alcohol dehydrogenase	*D. melanogaster*	NAD^+ → $NADP^+$	D38Q	510	54
D-lactate dehydrogenase	*L. delbrueckii*	NAD^+ → $NADP^+$	D175A	43	35
dihydrolipoamide dehydrogenase	*E. coli*	NAD^+ → $NADP^+$	7 mutations[a]	NA	36
isopropylmalate dehydrogenase	*T. thermophilus*	NAD^+ → $NADP^+$	9 mutations + insertion[b]	84100	55
leucine dehydrogenase	*T. intermedius*	NAD^+ → $NADP^+$	D203A+I204R+D210R	NA	34
formate dehydrogenase	*S. cerevisiae*	NAD^+ → $NADP^+$	D196A+ Y197R	2500000	56
ferredoxin:$NADP^+$ reductase	*A. sp. PCC 7119*	$NADP^+$ → NAD^+	S223D	8133	18
HMG-CoA reductase	*P. mevalonii*	NADPH → NADH	D146A+L148R	83300	57
nitrate reductase	*N. crassa*	NADPH → NADH	S920D+R932S	73000	16
cytochrome P450 reductase	*R. norvegicus*	NADPH → NADH	S596D	64290	17
glutathione reductase	*E. coli*	NADPH → NADH	7 mutations[c]	17700	58
ketol acid reductoisomerase	*E. coli*	NADPH → NADH	R68D+K69L+K75V+R76D	58100	59
p-hydroxybenzoate hydroxylase	*P. fluorescens*	NADPH → NADH	5 mutations[d]	50500	60
isocitrate dehydrogenase	*T. thermophilus*	$NADP^+$ → NAD^+	5 mutations[e]	120	61
isocitrate dehydrogenase	*E. coli*	$NADP^+$ → NAD^+	7 mutations[f]	1390000	62

[a] Fold improvement was calculated as $[(k_{cat}/K_m(NADPH))/(k_{cat}/K_m(NADH))]_{mutant}/[(k_{cat}/K_m(NADPH))/(k_{cat}/K_m(NADH))]_{wild-type}$ for NADH → NADPH and $[(k_{cat}/K_m(NADH))/(k_{cat}/K_m(NADPH))]_{mutant}/[(k_{cat}/K_m(NADH))/(k_{cat}/K_m(NADPH))]_{wild-type}$ for NADPH → NADH. NA = not determined in reference. [b] G185A/G189A/E203V/M204R/F205K/D206H/P210R. [c] S226R/D278K/I279Y/P324T/P325Y/G328E/G329R/S330L/A285V/ADGAKL insert between L330 and A331. [d] A179G/A183G/V197E/R198M/K199F/H200D/R204P. [e] R33S/Q34R/P35R/D36A/Y37E. [f] K283D/Y284I/N287G/V288I/I290A. [g] C201I/K344D/Y345I/V351A/Y391K/R395S/C332Y.

(*34*) to a low of a 43-fold change in $NADP^+$ utilization by *L. delbrueckii* D-lactate dehydrogenase (*35*). However, it should be noted that studies of other pyridine nucleotide-utilizing enzymes, such as *E. coli* dihydrolipoamide dehydrogenase (*36*), may have been more efficient but were not quantifiable due to the absence of any detectable activity of the native enzyme with the nonphysiological form of the coenzyme. The results suggest that, in general, more effective alterations in pyridine nucleotide specificity have been achieved when engineering a change in the $NADP^+$(H) to NAD^+(H) specificity of the various enzymes, indicating that mutagenesis of specific amino acid side chain residues to decrease the affinity for a somewhat larger substrate molecule via steric hindrance or for one possessing an additional, negatively charged moiety by charge stabilization has been more efficient.

Within the FNR family of flavoprotein oxidoreductases, specificity changes have been probed for FNR (*18*), cytochrome P450 reductase (*17*, *37*), the flavin domain of assimilatory nitrate reductase (*16*, *38*), and, as reported here, cytochrome b_5 reductase. Within this group, the flavin domain of nitrate reductase, which shares the highest degree of sequence conservation with the diaphorase domain of CB5R, is the only example of pyridine nucleotide coenzyme studies that have examined both NADPH- and NADH-specific isoforms of the enzyme (*16*, *38*). For nitrate reductase, mutagenesis of two residues, S920 and R932 in the NADPH-specific isoform, which are equivalent to D239 and F251 in rat CB5R, resulted in a (7.3×10^4)-fold switch in nucleotide specificity whereas substitutions of the same residues in the NADH-specific isoform resulted in only a (6.2×10^3)-fold alteration in specificity, clearly reinforcing the suggestion that additional amino acid residues should be considered when attempting to alter pyridine nucleotide specificity. Similarly, in CPR and FNR, residues distant from the pyridine nucleotide 2′ binding site have been shown to confer varying degrees of specificity (*18*, *37*). One notable example is the *re*-face stacking aromatic side chain of residue W676 of human CPR, a residue which has no structural equivalent in CB5R or NR due to differences in the alignment of the individual NADH binding and FAD binding domains. Döhr et al. (*37*) have reported an improvement in CPR NADH specificity of ~1000-fold when W676 was replaced by alanine. More recently, an endogenous fusion protein variant of rat CB5R has been reported (*20*) that is comprised of both the heme domain of cytochrome b_5 and the flavin domain of cytochrome b_5 reductase and that exhibits a marked preference for NADPH as the reducing substrate. Directed mutagenesis of selected residues, such as S422 and R437, within this enzyme may provide a further example of the efficiency of altering NAD(P)H specificity among flavoprotein transhydrogenases.

REFERENCES

1. Iyanagi, T., Watanabe, S., and Anan, K. F. (1984) *Biochemistry 23*, 1418−1425.
2. Strittmatter, P. (1965) *J. Biol. Chem. 240*, 4481−4487.
3. Hultquist, D. E., and Passon, P. G. (1971) *Nat. New Biol. 229*, 252−254.
4. Reddy, V., Kupfer, D., and Capsi, E. (1977) *J. Biol. Chem. 252*, 2797−2801.
5. Kitao, T., Sugita, Y., Yoneyama, Y., and Hattori, K. (1974) *Blood 44*, 879−884.
6. Hildebrant, A., and Estabrook, R. W. (1971) *Arch. Biochem. Biophys. 143*, 66−79.
7. Marohnic, C. C., and Barber, M. J. (2001) *Arch. Biochem. Biophys. 389*, 223−233.
8. Kimura, S., Hirokazu, N., and Takashi, I. (2001) *J. Biochem. 130*, 481−490.
9. Rossmann, M. G., Moras, D., and Olsen, K. W. (1974) *Nature 250*, 194−199.
10. Bewley, M. C., Marohnic, C. C., and Barber, M. J. (2001) *Biochemistry 40*, 13574−13582.
11. Karplus, P. A., Daniels, M. J., and Herriott, J. R. (1991) *Science 251*, 60−66.
12. Correl, C. C., Ludwig, M. L., Bruns, C. M., and Karplus, P. A. (1993) *Protein Sci. 2*, 2112−2133.
13. Yabusaki, Y., Murakami, H., and Ohkawa, H. (1988) *J. Biochem. 103*, 1004−1010.

14. Prosser, I. M., and Lazarus, C. M. (1990) *Plant Mol. Biol. 15*, 187−190.
15. Geller, D. A., Lowenstein, C. J., Shapiro, R. A., Nussler, A. K., DiSilvio, M., Wang, S. C., Nakayama, D. K., Simmons, R. L., Snyder, S. H., and Billiar, T. R. (1993) *Proc. Natl. Acad. Sci. U.S.A. 90*, 3491−3495.
16. Shiraishi, N., Croy, C., Kaur, J., and Campbell, W. H. (1998) *Arch. Biochem. Biophys. 358*, 104−115.
17. Elmore, C. L., and Porter, T. D. (2002) *J. Biol. Chem. 277*, 48960−48964.
18. Medina, M., Luquita, A., Tejero, J., Hermoso, J., Mayoral, T., Sanz-Aparicio, J., Grever, K., and Gomez-Moreno, C. (2001) *J. Biol. Chem. 276*, 11902−11912.
19. Zhu, H., Qiu, H., Yoon, H. W., Huang, S., and Bunn, H. F. (1999) *Proc. Natl. Acad. Sci. U.S.A. 96*, 14742−14747.
20. Davis, C. A., Dhawan, I. K., Johnson, M. K., and Barber, M. J. (2002) *Arch. Biochem. Biophys. 400*, 63−75.
21. Laemmli, U.K. (1970) *Nature 227*, 680−685.
22. Chen, G. C., and Yang, J. T. (1977) *Anal. Lett. 10*, 1195−1207.
23. Foust, G. P., Burleigh, B. D., Mayhew, S. G., Williams, C. H., and Massey, V. (1969) *Anal. Biochem. 27*, 530−535.
24. Sancho, J., and Gomez-Moreno, C. (1991) *Arch. Biochem. Biophys. 288*, 231−238.
25. Barber, M. J., Desai, S. K., and Marohnic, C. C. (2001) *Arch. Biochem. Biophys. 394*, 99−110.
26. Murataliev, M. B., and Feyereisen, R. (2000) *Biochemistry 39*, 5066−5074.
27. Kimura, S., Kawamura, M., and Iyanagi, T. (2003) *J. Biol. Chem. 278*, 3580−3589.
28. Massey, V. (1990) in *Flavins and Flavoproteins* (Curti, B., Ronchi, S., and Zanetti, G., Eds.) pp 59−67, Walter de Gruyter, Berlin.
29. Deng, Z., Aliverti, A., Zanetti, G., Arakaki, A. K., Ottado, J., Orellano, E. G., Calcaterra, N. B., Ceccarelli, E. A., Carrillo, N., and Karplus, P. A. (1999) *Nat. Struct. Biol. 6*, 847−53.
30. Iyanagi, T. (1977) *Biochemistry 16*, 2725−2730.
31. Iyanagi, T., Watanabe, S., and Anan, K. F. (1984) *Biochemistry 23*, 1418−1425.
32. Hermoso, J. A., Mayoral, T., Faro, M., Gomez-Moreno, C., Sanz-Aparicio, J., and Medina, M. (2002) *J. Mol. Biol. 319*, 1133−142.
33. Schoemaker, H. E., Mink, D., and Wubbolts, M. G. (2003) *Science 299*, 1694−1697.
34. Galkin, A., Kulakova, L., Ohshima, T., Esaki, N., and Soda, K. (1997) *Protein Eng. 10*, 687−690.
35. Chen, Z., Lee, W. R., and Chang, S. H. (1991) *Eur. J. Biochem. 202*, 263−267.
36. Bernard, N., Johnsen, K., Holbrook, J. J., and Delcour, J. (1995) *Biochem. Biophys. Res. Commun. 208*, 895−900.
37. Döhr, O., Paine, M. J. I., Friedberg, T., Roberts, G. C. K., and Wolf, C. R. (2001) *Proc. Natl. Acad. Sci. U.S.A. 98*, 81−86.
38. Barber, M. J. (2000) *FASEB J. 14*, A1416.
39. Thompson, J. D., Gibson, T. J., Plewniak, F., Jeanmougin, F., and Higgins, D. G. (1997) *Nucleic Acids Res. 24*, 4876−4882.
40. Pietrini, G., Carrera, P., and Borgese, N. (1988) *Proc. Natl. Acad. Sci. U.S.A. 85*, 7246−7250.
41. Shiraishi, N., Kubo, Y., Takeba, K., Kiyota, S., Sakano, K., and Nakagawa, H. (1991) *Plant Cell Physiol. 32*, 1031−1038
42. Nomura, Y., Nakagawa, M., Ogawa, N., Harashima, S., and Oshima, Y. (1992) *J. Ferment. Bioeng. 74*, 333−344.
43. Blattner, F. R., Plunkett, G., III, Bloch, C. A., Perna, N. T., Burland, V., Riley, M., Collado-Vides, J., Glasner, J. D., Rode, C. K., Mayhew, G. F., Gregor, J., Davis, N. W., Kirkpatrick, H. A., Goeden, M. A., Rose, D. J., Mau, B., and Shao, Y. (1997) *Science 277*, 1453−1474.
44. Friemann, A., Brinkmann, K., and Hachtel, W. (1991) *Mol. Gen. Genet. 227*, 97−105.
45. Long, D. M., Oaks, A., and Rothstein, S. J. (1992) *Physiol. Plant. 85*, 561−566.
46. Okamoto, P. M., and Marzluf, G. A. (1993) *Mol. Gen. Genet. 240*, 221−230.
47. Deng, Z., Aliverti, A., Zanetti, G., Arakaki, A. K., Ottado, J., Orellano, E. G., Calcaterra, N. B., Ceccarelli, E. A., Carrillo, N., and Karplus, P. A. (1999) *Nat. Struct. Biol. 6*, 847−853.
48. Porter, T. D., and Kasper, C. B. (1985) *Proc. Natl. Acad. Sci. U.S.A. 82*, 973−977.
49. Janssens, S. P., Shimouchi, A., Quertermous, T., Bloch, D. B., and Bloch, K. D. (1992) *J. Biol. Chem. 267*, 14519−14522.
50. Ostrowski, J., Barber, M. J., Rueger, D. C., Miller, B. E., Siegel, L. M., and Kredich, N. M. (1989) *J. Biol. Chem. 264*, 15796−15808.
51. Nishiyama, M., Birktoft, J. J., and Beppu, T. (1993) *J. Biol. Chem. 268*, 4656−4660.
52. Holmberg, N., Ryde, U., and Bülow, L. (1999) *Protein Eng. 12*, 851−856.
53. Clermont, S., Corbier, C., Mely, Y., Gerard, D., Wonacott, A., and Branlant, G. (1993) *Biochemistry 32*, 10178−10184.
54. Bocanegra, J. A., Scrutton, N. S., and Perham, R. N. (1993) *Biochemistry 32*, 2737−2740.
55. Chen, R., Greer, A., and Dean, A. M. (1996) *Proc. Natl. Acad. Sci. U.S.A. 93*, 12171−12176.
56. Serov, A. E., Popova, A. S., Fedorchuk, V. V., and Tishkov, V. I. (2002) *Biochem. J. 367*, 841−847.
57. Friesen, J. A., Lawrence, C. M., Stauffacher, C. V., and Rodwell, V. W. (1996) *Biochemistry 35*, 11945−11950.
58. Scrutton, N. S., Berry, A., and Perham, R. N. (1990) *Nature 343*, 38−43.
59. Rane, M. J., and Calvo, K. C. (1997) *Arch. Biochem. Biophys. 338*, 83−89.
60. Eppink, M. H. M., Overkamp, K. M., Schreuder, H. A., and Van Berkel, W. J. H. (1999) *J. Mol. Biol. 292*, 87−96.
61. Yaoi, T., Miyazaki, K., Oshima, T., Komukai, Y., and Go, M. (1996) *J. Biochem. 119*, 1014−1018.
62. Chen, R., Greer, A., and Dean, A. M. (1995) *Proc. Natl. Acad. Sci. U.S.A. 92*, 11666−11670.

BI034819B